Available online at www.sciencedirect.com
ScienceDirect
Trans. Nonferrous Met. Soc. China 21(2011) 2396−2401
Transactions of Nonferrous Metals Society of China
www.tnmsc.cn

Adiabatic shear fracture in Ti−6Al−4V alloy

ZHANG Jing[1], TAN Cheng-wen[1, 2], REN Yu[1], YU Xiao-dong[1],
MA Hong-lei[2], WANG Fu-chi[1], CAI Hong-nian[1]

1. School of Material Science and Engineering, Beijing Institute of Technology, Beijing 100081, China;
2. Laboratory of Advanced Materials Behavior Characteristics,
China Astronaut Research and Training Center, Beijing 100081, China

Received 29 October 2010; accepted 16 May 2011

Abstract: Separated specimens of Ti−6Al−4V alloy were dynamically loaded at a strain rate of 3 900 s^{-1} using a split Hopkinson pressure bar (SHPB) apparatus. The fracture features of the separated specimens were investigated by a scanning electron microscope. The results show that adiabatic shear failure occurs in the tested specimens, and two typical areas (dimple and smooth areas) with different features are alternatively distributed on the whole fracture surface. The dimple areas originate from voids generation and coalescence, exhibiting ductile fracture characteristics. Simultaneously, ultrafine grains (UFGs) and microcracks among grains are observed on the smooth areas, indicating that the emergence of UFG areas is caused by the propagation of microcracks along grain boundaries and exhibits brittle fracture characteristics. Fracture occurring in adiabatic shear bands is not uniform and ultimate rupture is resulted from ductile and brittle fracture modes.
Key words: Ti−6Al−4V; adiabatic shear; dynamic fracture mode

1 Introduction

Adiabatic shear bands (ASBs) are frequently formed in metals in a wide range of deformation at high strain rates, e.g., hypervelocity impact, penetration and high-speed machining [1−5]. In general, ASBs are considered narrow bands of intense plastic shear strain embedded in a homogeneously deformed region. A lot of investigations concerning ASBs of titanium and its alloys have been carried out [6]. MEYERS et al [7−8] investigated evolution of microstructure in titanium and titanium alloys and found dynamic recrystallization occurring in ASBs. CHICHILI et al [9] observed the presence of the new nanocrystalline grains formed inside ASBs in α-Ti examined using the compression−torsion Kolsky bar. The results of the submicron grains observed are in agreement with the early TEM observation by GREBE et al [10] for Ti−6Al−4V alloy. Generally, formation of ASBs is considered a failure mechanism of impacted materials. Nevertheless, the deformed body keeps its integrity if no cracks are generated because ASBs adhere to the matrix materials. Hence, fracture in ASBs is the essential reason inducing failure of impacted materials, which should be considered. Efforts have been made to study the transition from adiabatic shear banding to fracture under high strain rate condition. In our previous research [11−12], many fracture surfaces were observed in specimens by ballistic tests, in which specimens deformed very quickly at strain rates higher than 10^4 s^{-1}. At such high strain rates, most fracture surfaces are smeared by segments separated from specimens. It is hard to accurately investigate the fresh surface and analyze the fracture mode occurred in ASBs. Thus, dynamic fracture mode of materials is not accurately illustrated under high strain rate condition, namely, transition from formation of ASBs to fracture is not clear. In this study, a way to obtain the fracture surface was proposed at a relatively low strain rate of 3 900 s^{-1} and the fracture mode under dynamic condition was analyzed. The results provide new experimental evidence and insights of fracture mode in ASBs of impacted Ti−6Al−4V alloy.

2 Experimental

The material studied was conventional Ti−6Al−4V alloy. Dynamic compression tests at a strain rate of 3 900 s^{-1} were performed using a split Hopkinson pressure bar apparatus. Based on the previous experience,

Corresponding author: TAN Cheng-wen; Tel: +86-10-68912712; Fax: +86-10-62890250; E-mail: tanchengwen@126.com
DOI: 10.1016/S1003-6326(11)61026-1

the specimens of Ti−6Al−4V alloy did not rupture completely and two parts were bonded together in uniaxial dynamic compression test, leading to additional difficulty in investigating fracture surface of titanium alloys at a strain rate of 10^3 s^{-1}. In other study [13], adiabatic shear localization was sensitive to the fiber orientation and the intensity of adiabatic shear localization increases with increasing angle between loading direction and fiber direction. A narrower adiabatic shear localization zone can be obtained when loaded at an angel of 45° with respect to the fiber orientation than that obtained when the loading axial was parallel to the fiber orientation. It was easier to obtain completely ruptured specimens and observe adiabatic shear fracture surface to analyze the fracture mode in ASBs. So, the as-received Ti−6Al−4V alloy was fabricated by uniaxial forging to gain microstructure with obvious fiber pattern. Figure 1(a) shows the microstructure of the forging bars, consisting of predominant α phase, and the average aspect ratio is approximately 4.

The cylindrical specimen (d5 mm×5 mm) for uniaxial dynamic compression was cut along the angle of 45° between the cylinder axial direction and initial rod axial direction. The sketch inserted in Fig. 1(a) is the schematic diagram of the specimen machined 45° to the axial direction from the forged bar. After dynamic compressive tests, the specimens were entirely split, as displayed in Fig. 1(b). The tested specimen was carefully recovered and rinsed in acetone to clean the fracture surfaces. The JEM−200CX transmission electron microscope (TEM) was applied to investigate the microstructure adjacent to the fracture surface. The Quanta 200F field emitting scanning electron microscopy (FE−SEM) was employed to investigate the pattern of fracture surface. The zone observed was the center of the fracture surface.

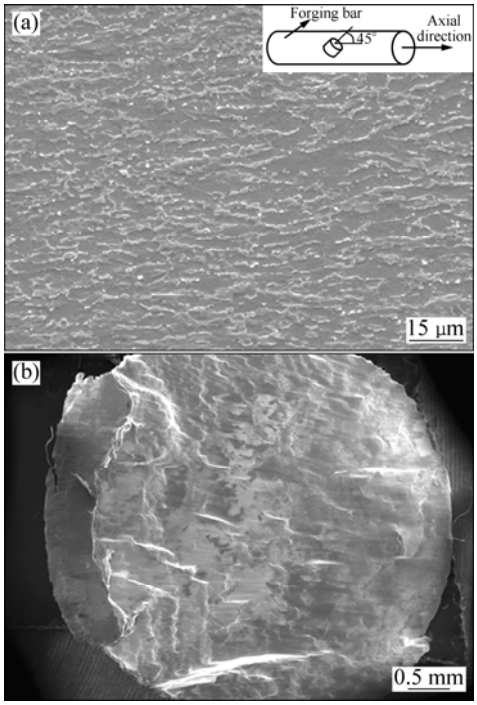

Fig. 1 SEM images of forged bar (a) and recovered specimen after dynamic compression (b) (Insert: schematic illustration of specimens machined from forged bar)

3 Results

3.1 Dynamic mechanical behaviors

The dynamic compression stress—strain curve at strain rate of 3 900 s^{-1} is shown in Fig. 2. It is obvious that the flow stress becomes steady as the stress exceeds the dynamic yield strength to about 1 600 MPa. This fact is attributed to the thermal softening under dynamic loading conditions, which counteracts the strain hardening and strain rate hardening. When the thermal softening effect exceeds the two hardening effects, the flow stress decreases rapidly, corresponding to the unloading stage in Fig. 2.

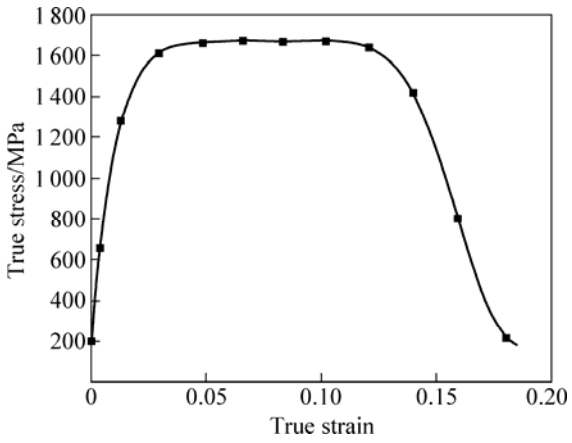

Fig. 2 Dynamic compression true stress—strain curve at strain rate of 3 900 s^{-1}

3.2 Microstructures

Figure 3 shows the microstructure pattern adjacent to the fracture surface in the tested specimen. It is apparently found that adiabatic shear failure occurs in Ti−6Al−4V alloy during the dynamic compression test, and the same phenomenon was observed during Taylor tests and ballistic tests [14−15], and the formed ASB is parallel to the fiber direction. Moreover, cracks propagate along the adiabatic shear band in a rupture of the specimen, as shown in Fig. 3(a). Figure 3(b) shows the microstructure of the ASB, which exhibits a large number of equiaxed UFGs with size of 100−500 nm approximately. The image of the selected area diffraction (SAD), insert of Fig. 3(b), shows the that the dynamic recrystallization occurs truly in the formation process of

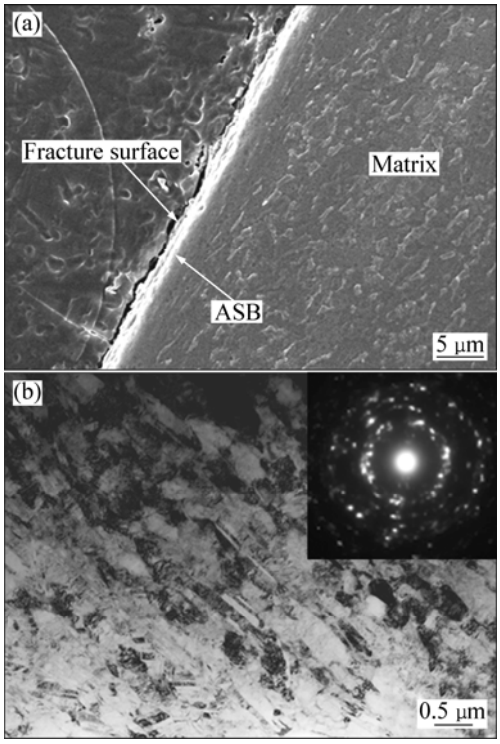

Fig. 3 SEM and TEM images of tested specimen: (a) SEM image showing ASB adjacent to fracture surface; (b) TEM image showing microstructure within ASB

ASB in Ti−6Al−4V alloy. Additionally, there is no clear evidence to suggest that the material within the ASB undergoes a phase transformation, which is consistent with the results in Ref. [16].

3.3 Fractography

Figure 4 shows the SEM images of the fracture surface of the tested specimen at strain rate of 3 900 s^{-1} at various magnifications. As displayed in Fig. 4(a), the fracture surfaces *A* and *B* are classified into two main areas, ductile dimples areas and relative smooth areas, respectively. Figures 4(b) and (c) present the fractography of *A* and *B* at higher magnification, respectively. Figure 4(b) shows the ductile dimples areas, along the maximum shear stress direction and there are elongated dimples, which indicates that large plastic deformation takes place in ASB. In contrast of the dimples areas, the size of the UFGs is 100−500 nm, which is much smaller than that of the initial α grains, distributing on one smooth area as displayed in Fig. 4(c). It is noted that the size of the UFGs is almost consistent with that observed by TEM, suggesting that the UFGs of the fracture surface might be recrystallized grains. Furthermore, microcracks and microvoids are also observed on the smooth surface.

According to previous viewpoints [16−17], smooth areas are caused by rubbing between the fragment and

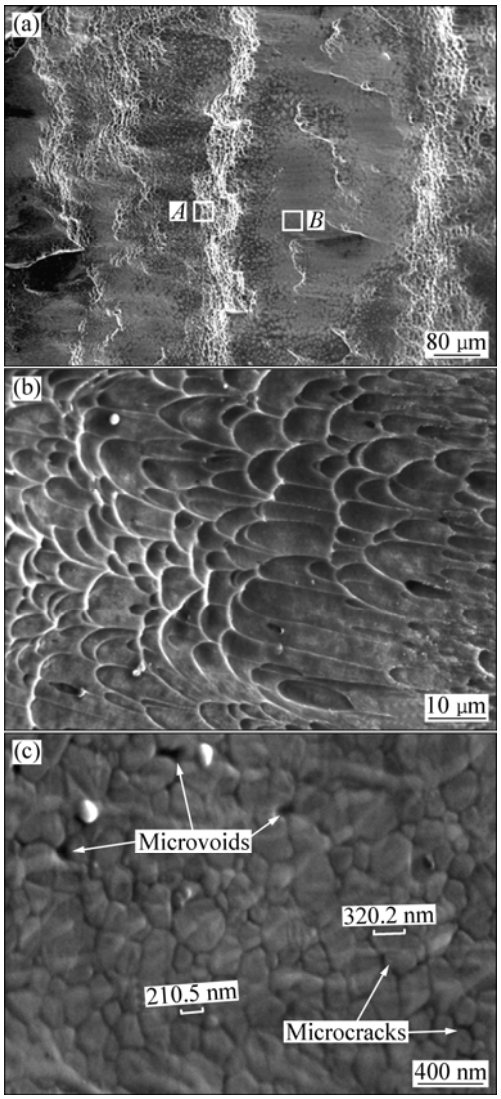

Fig. 4 SEM images of fracture surface at lower magnification (a), dimple area (b), ultrafine grains area (c) in tested specimens

the fracture surface. If this hypothesis is reasonable, it is impossible that a large amount of UFGs are distributed on the fracture surface. Hence, the smooth area is fresh, rather than smeared, in the ruptured specimen. As displayed in Fig. 3(a), the separation of specimen is attributable to the fracture propagating along the adiabatic shear band. Therefore, the patterns of the fracture surface should reflect the information of ASB.

4 Discussion

As shown in Figs. 3(b) and 4(c), dynamic recrystallization occurs reliably within the ASB. Therefore, it is suggested that the UFGs should be formed via dynamic recrystallization mechanism which is firstly postulated and described in increasing details by ANDRADE et al [18].

In essence, one begins with a random dislocation distribution, which is not a low-energy configuration. This random distribution gives way to elongated cells. As the deformation continues and the misorientation increases, these cells become elongated subgrains, which are plastically deformed in turn, leading to further breakup. Eventually, the elongated subgrains break up into approximately equiaxed ultrafine grains. Once this equiaxed ultrafine-grain structure is achieved, it has to undergo additionally plastic deformation under the sequent loading condition. When the grain size is reduced to the submicron range, the deformation mechanisms operating at conventional grain size may change. The rotation of grain boundaries leads to the equiaxed grains formed in ASBs [19]. A gradual derivation of grain boundary rotation is provided by NESTERENKO et al [20], which can be described as:

$$\frac{\tan\theta-\frac{2}{3}\cos\theta}{1-2\sin\theta}+\frac{4}{3\sqrt{3}}\ln\frac{\tan\frac{\theta}{2}-2-\sqrt{3}}{\tan\frac{\theta}{2}-2+\sqrt{3}}+\cdots+\frac{2}{3}-\frac{4}{3\sqrt{3}}\ln\frac{2+\sqrt{3}}{2-\sqrt{3}}=\frac{4\delta D\gamma}{L_1kT}t \quad (1)$$

where θ is the rotation angle of grain boundary; t is the time of rotation; δ is the grain boundary thickness (6.0×10^{-10} m); D is a constant correlated with the grain boundary diffusion (1×10^{-5} m^2/s); γ is the grain boundary energy (1.19 J/m^2); k is a constant (1.38×10^{-23} J/K), T is temperature. From Eq. (1), temperature T is the uppermost factor for the reorientation of grain boundary. Under dynamic loading condition, the adiabatic temperature rising during the course of dynamic loading can be calculated as:

$$\Delta T=\frac{\eta}{\rho c_V}\int\tau\mathrm{d}\gamma \quad (2)$$

where β is the Taylor-Quinney coefficient which characterizes the portion of plastic work converted into heat (assumed to be 0.9 in this case); ρ is the density (4.4 g/cm^3); c_V is the special heat capacity (0.204 J/(g·K)); τ is the shear stress; γ is the true shear strain. It is obvious that the flow stress is steadily 1 600 MPa, as shown in Fig. 2. The shear strain with the ASB is estimated by measuring the geometry of the elongated dimples, and the estimated shear strain is 3−4. So, the estimated temperature rising with the ASB of Ti−6Al−4V alloy is (0.5−0.6)T_m (T_m is the melt temperature, 1 888 K in this case). Here, temperature T is evaluated to 0.5T_m and the diameter of subgrain L_1 is assumed to 0.2, 0.3, 0.4 and 0.5 μm, respectively. The rate of the rotation decreases with increasing θ and gradually approaches 30° as $t\to\infty$. The calculation results shown in Fig. 5 predict the rotations of the boundary within the deformation time (approximately 10 μs) at 0.5T_m for subgrain sizes of 0.2−0.5 μm. It is found that 30° orientation of grain boundaries completes within several μs. Although this does not exclude the probability of reorientation or accommodation of the grain boundaries during cooling, the reorientation of grain boundaries can take place during plastic deformation. It is testified that the UFGs-like patterns distributing on the fracture surface potentially are caused by dynamic recrystallization in the tested specimens.

From Fig. 4(a), it is interesting to note that the smooth areas and the dimple areas are emerged alternately on the fracture surface along the shear direction. This phenomenon indicates that different fracture modes might take place in the same adiabatic band (or plane). In general, the fracture modes are correlated with temperature and strain rate. Metals show more brittle with decreasing temperature or increasing strain rate [21]. Thus, competition between thermal softening owing to temperature rise and strain rate dependence influences the fracture mode that occurs in ASBs under dynamic loading condition. In one test, the strain rate can be considered a constant in one ASB. Thus, temperature becomes a main factor influencing the fracture mode in ASB. Distribution of temperature in ASB has been investigated. GUDURU et al [22] investigated ASBs using high speed optical and infrared diagnostics and found that a shear band showed non-uniform temperature distribution along the length of the band. LI et al [23] and TENG et al [24] also confirmed the non-uniform temperature distribution and found that the temperature distribution has periodic patterns in both space and time by means of numerical computation, which is plausible to have some influence on the failure mechanism.

Therefore, it is proposed that periodic temperature distribution induces possibly the interval emergence of dimple areas and smooth areas. Furthermore, TENG et al

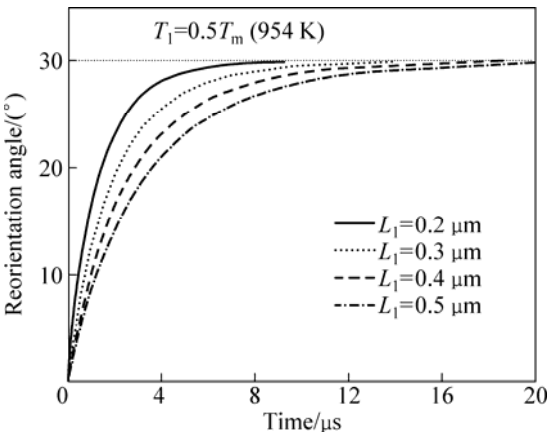

Fig. 5 Time vs reorientation angel with various grain sizes

[24] even revealed “hot spots” distributed periodically along the length of a well-developed shear band. At these hot spots, because thermal softening is predominant over strain rate hardening, voids firstly nucleate and then coalescence occurs with elongation of the voids and ligaments bridging the voids. This leads to the formation of a fracture surface consisting of elongated dimples. It represents typical ductile fracture characteristics. In contrast to the dimple areas, microcracks and microvoids appear in the smooth areas. Separation of UFGs from materials within the ASB leads to the formation of microvoids, which is attributed to the propagation of the microcracks along the UFG boundaries. This phenomenon exhibits typical brittle fracture characteristics. The reason is that the effect of thermal softening owing to temperature rise is less than that of strain rate at a place at relatively low temperature of ASB. Figure 6 shows the schematic illustration of dimples coalescence of voids and cracks propagating along grain boundaries which induce completely fracture. Actually, fracture occurs uniformly in ASBs and two different fracture modes (ductile and brittle fracture) in ASB of Ti−6Al−4V alloy are coexistent under dynamic loading condition. It is noted that more experiments should be done to verify the universality of the dynamic fracture mode in other materials.

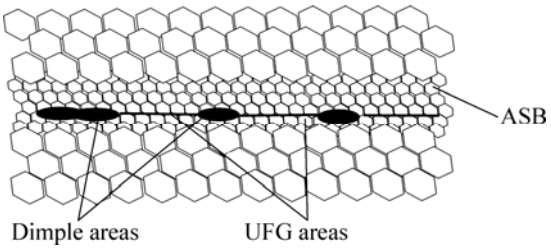

Fig. 6 Schematic illustration of dimples areas and UFG areas within ASB

5 Conclusions

1) Separated specimens of Ti−6Al−4V alloy are obtained at strain rate of 3 900 s^{-1} using SHPB apparatus and complete rupture occurrs along ASB. Two different features on fracture surface, namely dimple areas and UFG areas, are observed by SEM. The UFGs within the ASB with size in a range of 200−500 nm, form during dynamic recrystallization.

2) Since the temperature distribution is periodic in ASBs, different fracture modes exist in transition from adiabatic shear banding to fracture. Temperature rise in ASBs causes the generation of voids and then the voids are transformed into elongated dimples that exhibit typical ductile fracture characteristics.

3) In contrast, the UFG areas are formed by the cracks propagating along grain boundaries which exhibit brittle fracture characteristics. It is evident that two fracture modes, ductile fracture and brittle fracture, coexist in ASB of Ti−Al−4V alloy under dynamic loading condition.

References

[1] NESTERENKO V F, MEYERS M A, WRIGHT T W. Self-organization in the initiation of adiabatic shear bands [J]. Acta Mater, 1998, 46(1): 327−340.

[2] XU Y B, ZHONG W L, CHEN Y J. Shear localization and recrystallization in dynamic deformation of 8089 Al-Li alloy [J]. Mater Sci Eng A, 2001, 299(1−2): 287−295.

[3] XUE Q, MEYERS M A, NESTERENKO V F. Self-organization of shear bands in titanium and Ti-6A1-4V alloy [J]. Acta Mater, 2002, 50(3): 575−596.

[4] DUFFY J, CHI Y C. On the measurement of local strain and temperature during the formation of adiabatic shear bands [J]. Mater Sci Eng A, 1992, 157(2): 195−210.

[5] SCHOENFELD S E, BIMAL K. Texture effects on shear response in Ti-6Al-4V plates [J]. Int J Plast, 2002, 18(4): 461−486.

[6] XU Y B, BAI Y L, MEYERS M A. Deformation, phase transformation and recrystallization in the shear bands induced by high-strain rate loading in titanium and its alloys.[J] J Mater Sci Technol, 2006, 22(6): 737−746.

[7] MEYERS M A, SUBHASH G, KAD B K, PRASAD L. Evolution of microstructure and shear band formation in α-hcp titanium [J]. Mechanics of Materials, 1994, 17(2−3): 175−193.

[8] MEYERS M A, XU Y B, XUE Q, PEREZ-PRADO M T, MCNELLEY T R. Microstructural evolution in adiabatic shear localization in stainless steel [J]. Acta Mater, 2003, 51(5): 1307−1325.

[9] CHICHILI D R, RAMESH K T, HEMKER K J. Adiabatic shear localization in α-titanium: Experiments, modeling and microstructural evolution [J]. J Mech Phys Solids, 2004, 52(8): 1889−1909.

[10] GREBE H A, PAK H R, MEYERS M A. Adiabatic shear localization in titanium and Ti-6 pct Al-4 pct V alloy [J]. Metall Trans A, 1985, 16(5): 761−775.

[11] LIU X Q, TAN C W, ZHANG J, HU Y G, MA H L, WANG F C, CAI H N. Influence of microstructure and strain rate on adiabatic shearing behavior in Ti-6Al-4V alloys [J]. Mater Sci Eng A, 2009, 501(1−2): 30−36.

[12] REN Y, TAN C W, ZHANG J, WANG F C. Dynamic fracture of Ti−6Al−4V alloy in the Taylor impact test [J]. Transactions of Nonferrous Metals Society of China, 2001, 21(2): 223−235.

[13] LIU J X, LI S K, FAN A L, SUN H C. Effect of fibrous orientation on dynamic mechanical properties and susceptibility to adiabatic shear band of tungsten heavy alloy fabricated through hot-hydrostatic extrusion [J]. Mater Sci Eng A, 2008, 487(1−2): 235−242.

[14] LI G A, ZHEN L, LIN C, GAO R S, TAN X, XU C Y. Deformation localization and recrystallization in TC_4 alloy under impact condition [J]. Mater Sci Eng A, 2005, 395(1−2): 98−101.

[15] ME-BAR Y, ROSENBERG Z. On the correlation between the ballistic behavior and dynamic properties of titanium-alloy plates [J]. Int J Impact Eng, 1997, 19(4): 311−318.

[16] LIAO S C, DUFFY J. Adiabatic shear bands in a Ti−6Al−4V titanium alloy [J]. J Mech Phys solids, 1998, 46(11): 2201−2231.

[17] RITTEL D, WANG Z G. Thermo-mechanical aspects of adiabatic shear failure of AM50 and Ti6Al4V alloys [J]. Mechanics of Materials, 2008, 40(8): 629−635.

[18] ANDRADE U R, MEYERS M A,VECCHIO K S, CHOKSHI A H. Dynamic recrystallization in high-strain, high-strain-rate plastic

deformation of copper [J]. Acta Metall mater, 1994, 42(9): 3183.
[19] KUHLMANN-WILSDORF D, HANSEN N. Geometrically necessary, incidental and subgrain boundaries [J]. Scripta Metall Mater, 1991, 25(7): 1557−1562.
[20] NESTERENKO V F, MEYERS M A, LASALVIA J C, BONDAR M P, CHEN Y J, LUKYANOV Y L. Shear localization and recrystallization in high-strain, high-strain-rate deformation of Tantalum [J]. Mater Sci Eng A, 1997, 229(1−2): 23−41.
[21] XU Z, LI Y. Dynamic behaviors of 0Cr18Ni10Ti stainless steel welded joints at elevated temperatures and high strain rates [J]. Mechanics of Materials, 2009, 41(2): 121−130.
[22] GUDURU P R, ROSAKIS A J, RAVICHANDRAN G. Dynamic shear bands: An investigation using high speed optical and infrared diagnostics [J]. Mechanics of Materials, 2001, 33(7): 371−402.
[23] LI S F, LIU W K, QIAN D, GUDURU P R, ROSAKIS A J. Dynamic shear band propagation and micro-structure of adiabatic shear band [J]. Comput Methods Appl M, 2001, 191(1−2): 73−92.
[24] TENG X, WIERZBICKI T, COUQUE H. On the transition from adiabatic shear banding to fracture [J]. Mechanics of Materials, 2007, 39(2): 107−125.

Ti−6Al−4V 合金中的绝热剪切断裂

张 静[1]，谭成文[1,2]，任 宇[1]，于晓东[1]，马红磊[2]，王富耻[1]，才鸿年[1]

1. 北京理工大学 材料学院，北京 100081；
2. 中国航天员科研与训练中心 先进材料行为特性实验室，北京 100081

摘 要：利用分离式霍普金森压杆(SHPB)装置在 3 900 s^{-1} 应变率条件下对 Ti−6Al−4V 合金进行动态加载，获得完全分离的断裂试样。使用扫描电子显微镜对试样的断裂特征进行观察。结果表明：试样中出现绝热剪切断裂，试样断口上交替分布着两个不同特征的典型区域(韧窝区及平滑区)。其中，韧窝区由微孔洞形核、长大并最终连接形成，表现出韧性断裂特征。在平滑区观察到超细晶粒(UFGs)，且晶粒间可观察到微裂纹，说明平滑区由微裂纹沿晶界扩展形成，表现出脆性断裂特征。由此可知，Ti−6Al−4V 合金在动态加载过程中沿绝热剪切带发生的断裂失效过程不均匀，韧性及脆性两种断裂模式的共同作用导致该合金样品的最终断裂。

关键词：Ti−6Al−4V 合金；绝热剪切带；动态断裂模式

(Edited by FANG Jing-hua)